International Journal of Mathematical, Engineering and Management Sciences
Vol. 9, No. 5, 1019-1034, 2024
https://doi.org/10.33889/IJMEMS.2024.9.5.053

Ram Arti Publishers

Improved Reduced Switch Converter Topology for Torque Ripple Reduction in Four-Phase Switched Reluctance Motor Under Dynamic Loading

Ritika Asati
Department of Electrical Engineering,
Bharati Vidyapeeth (Deemed to be) University, College of Engineering, Pune, Maharashtra, India.
E-mail: ritikaasati86@gmail.com

Deepak S. Bankar
Department of Electrical Engineering,
Bharati Vidyapeeth (Deemed to be) University, College of Engineering, Pune, Maharashtra, India.
E-mail: dsbankar@bvucoep.edu.in

Vinay Kumar Jadoun
Department of Electrical & Electronics Engineering,
Manipal Institute of Technology, Manipal Academy of Higher Education, Manipal, Karnataka, India.
E-mail: vinay.jadoun@manipal.edu

Majed A. Alotaibi
Department of Electrical Engineering,
College of Engineering, King Saud University, Riyadh, Saudi Arabia.
E-mail: MajedAlotaibi@ksu.edu.sa

Hasmat Malik
Department of Electrical Power Engineering,
Faculty of Electrical Engineering, Universiti Teknologi Malaysia, Skudai, Johor, Malaysia.
&
Department of Electrical Engineering,
Graphic Era (Deemed to be University), 248002, Dehradun, Uttarakhand, India.
E-mail: hasmat.malik@gmail.com

Fausto Pedro García Márquez
Ingenium Research Group,
Universidad Castilla-La Mancha, 13071, Ciudad Real, Spain.
E-mail: faustopedro.garcia@uclm.es

(Received on December 10, 2023; Revised on March 6, 2024 & March 28, 2024; Accepted on April 22, 2024)

Abstract
In this paper, simulation, and performance comparison of a switched reluctance motor (SRM) for a classical asymmetric bridge converter and an improved reduced switch converter topology are provided. In an improved converter, switches are shared by adjacent phases, and one diode is connected in series with each phase winding to avoid reversal of current. Double-phase magnetization is adopted for the analysis of both converter topologies. The performance of both converter topologies are demonstrated using a proportional plus integral (PI) based hysteresis current controller and dynamic load on a 7.5 kW, 8/6 pole, 4-phase SRM. Improved reduced switch converter topology uses half the number of switches as compared to the classical asymmetric bridge converter. According to the simulation results, an improved converter offers superior starting and average torque with less speed settling time. An improved converter reduces the most serious problem of torque ripple in SRM by 50% compared to the classical topology. The reduced switches lower the winding losses and improve the efficiency of the drive system.

Keywords- Switched reluctance motor (SRM) drive, Asymmetric bridge converter (ABC), Reduced switch converter, Electric Vehicle (EV), Torque ripple.

1. Introduction

Across the world, various innovations are going on in the field of electric motors that are compatible with dynamic load applications like electric vehicles (EVs). EVs need a motor that is compact in size, low in cost, easy to manufacture, and has the capability to work at high speed in harsh environments (Ma et al., 2019). Commonly used electric motors for EVs use permanent magnets and it is difficult to drive such motors in the region of high speed due to the presence of permanent magnets on the rotor. Also, the manufacturing cost of a permanent magnet motor is high as it is not available in India and involves high cost of mining and refining (Padmanaban and Saravanan, 2023). A switched reluctance motor (SRM) is a rival to the many competing motors for dynamic load applications. Its rotor structure is rigid with no permanent magnet, no windings and brushes; making it low in weight and in size (Yi and Cai, 2016a). SRM doesn't have any air slot, which helps in making it simple to design and manufacture (Sun et al., 2023). Unfortunately, this motor suffers from torque ripple problem due to the singly-excited, doubly-salient structural design that adds up to a reduction in the overall average torque of SRM (Ho et al., 2019).

The block diagram of the SRM drive system is shown in **Figure 1**. It requires a power converter and a controller to operate and perform efficiently to give the maximum possible output (Mittal, 2023). A PI-based closed-loop control is employed here by continuously monitoring the speed using a position sensor (Al-Amyal et al., 2022). The load connected to the output of the motor is dynamic i.e., an electric vehicle. The most commonly used classical asymmetrical bridge converter (ABC) gives the best performance for dynamic load but uses two switches per phase (Mahmoud et al., 2013; Sun et al., 2019). A converter with fewer switching devices per phase can typically reduce the cost of the entire drive system. Constant research is going on for SRM converters having fewer switches per phase (Li et al., 2022). An Improved converter will help to overcome the limitations of conventional converter topologies and improve the overall performance during dynamic loading conditions. Mid-point converter, shared switch type converter, C-dump, C dump with freewheeling converter, and integrated multiport power converter (IMPC) are a few of the popular converters in the less switch per phase converter category addressed in the literature.

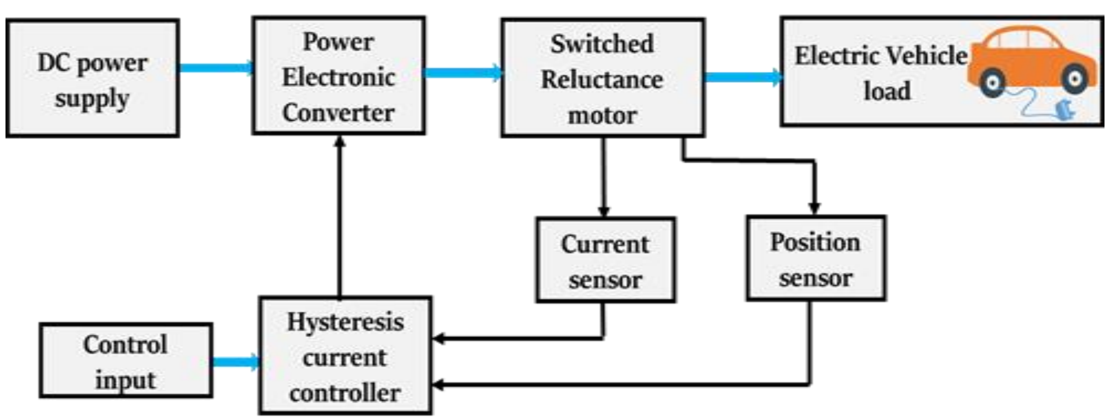

Figure 1. Block diagram of closed loop SR motor drive.

Split DC supply converter, another name for the midpoint converter uses only one switch and one diode per phase. The challenge of balancing the capacitor voltage in this converter is enormous, and the DC link capacitor has a significant current ripple (Han et al., 2021; Zhao and Ye, 2023). As the voltage appearing across the winding is half that of the source voltage, the speed obtained with this converter is reduced to half (Asati et al., 2023). In (Guan et al., 2020), a novel N+2 switch power converter topology that is very identical to split supply converter architecture is published. The two capacitors of the split converter are replaced with two switches in the middle. These spare switches undergo stress, reliability, and fault testing. However, a mid-point switch has a higher frequency of switching. Shared switch topology or Miller converter shares the switching device and diode in more than one phase and has the possibility of independent phase control (Son et al., 2021). The inability to turn on many phases at once, undesired circulating current, and phase current overlap at high speeds are some of the limitations (Pires et al., 2020). C-dump converter has fewer switches and phase control is independent. However, the voltage rating of the switch is twice as well as uses passive components in the dump circuit (Mehta et al., 2018; Riyadi, 2018). C-dump type with freewheeling overcomes the constraint of the C-dump type with enhanced output voltage freedom (Indira and Venmathi, 2023). Only motoring operation is feasible in this due to the lack of an energy recovery circuit (Cabezuelo et al., 2017; Krishnan, 2001). Integrated multiport power converter uses five switches for a four phase motor, widens speed range, reduces capacitor requirement, and less source current ripple (Cai and Yi, 2016). However, simple control technique limits its performance so advanced complicated control techniques are required to improve the system's performance, and expansibility (Subbamma et al., 2016; Yi and Cai, 2016b). A converter with less than two switches per phase is shown in (Pollock and Williams, 1990). The switches in this converter are connected to multiple motor phases, and the way these switches function affects the current flowing through each of the phases that are connected to them. Furthermore, it is challenging to raise the flux linkage in an adjacent phase while rapidly reducing it in the current phase. In (Ding et al., 2023) one diode and one switch are utilized in each phase of an x-type converter. The analysis is done on two freewheeling modes, and battery charging efficiency has reached 82% in these modes. Flyback converter are incorporated in a modular converter for quick demagnetization which is described in (Rana and Teja, 2020); the benefit of reduced torque ripple and fewer switches per phase are gained. However, the large discharge circuit limits the benefit of using fewer switches due to its bulky size.

The converter presented in the literature work may have fewer switches per phase, but only a few of the converter topologies have contributed towards improving the SRM limitation, i.e., torque ripple reduction for dynamic load. To reduce the total size of the converter unit and the number of switching devices in each phase, an improved reduced switch converter has been described in this research work. Analysis and study of an improved converter and classical asymmetric bridge converter have been carried out, based on the double-phase magnetization scheme. Between the magnetization and demagnetization states, a freewheeling state is added by this reduced switch converter design. In terms of average torque, high beginning torque, and settling time; an improved reduced switch converter outperforms even though it has half as many switches. Additionally, this converter lessens the main issue concerning torque ripple in SRM. The complete paper is systematized into different sections: In Section 2, fundamental equations of the SRM and the requirement for the SRM power converter unit have been reviewed; Section 3 explains the operation, important features, and conduction mode of both the new reduced switch converter and classical converter topology. Section 4 validates and compares the simulation findings of new and classical converters, and Section 5 concludes the simulation results.

2. SRM Fundamentals

This section is divided into two distinct subsections. The first part shows simplified expressions for power, electromagnetic torque, and torque ripples. These equations are useful in analyzing power converter performance. In the second part, the SRM power converter requirements are reviewed, which differ from the other motors due to the current polarity independence and negligible mutual coupling between phases.

2.1 Mathematical Equations of SRM

Switched reluctance motors are represented using linear mathematical modelling equations. A few of the main equations are voltage and torque equations. The formula for the voltage delivered to the phase winding of the SRM is represented by Equation (1) (Kumar et al., 2023):

$$V = Ri + L(\Theta, i)\frac{di}{dt} + \frac{dL(\Theta,i)}{d\Theta}\,\omega_m\, i \tag{1}$$

In Equation (1), V is the per phase applied voltage which supplies the resistive drop in motor winding (Ri), the second part is the voltage drop in motor winding inductance L, and the last term represents back emf produced in the winding. The mechanical power developed by the rotor is given by Equation (2) considering all mechanical losses are negligible (Kumar et al., 2023):

$$P_{mech} = \frac{i^2}{2}\frac{dL(\Theta,i)}{d\theta}\,\omega_m \tag{2}$$

Torque in an SRM is produced due to the excited stator poles and rotor poles alignment that gives maximum inductance. Equation (3) shows the instantaneous torque produced by SRM (Fang et al., 2021):

$$T_{inst} = \frac{P_{mech}}{\omega_m} = \frac{i^2}{2}\frac{dL(\Theta,i)}{d\theta} \tag{3}$$

From Equation (3), it can be inferred that:

- In SRM, the torque varies as a square of current but it is independent of the current direction in the phase winding.
- Torque is a function of the inductance of the phase winding that varies with the position of the rotor, making SRM a nonlinear motor.
- For motoring operation $\frac{dL(\Theta,i)}{d\Theta} > 0$ produces positive torque while during regeneration $\frac{dL(\Theta,i)}{d\Theta} < 0$ gives negative torque.
- For breaking torque generation, phases need to be energized in reverse sequence.
- By varying supply voltage, torque can be controlled as it changes the current proportionally.
- Commutation angle control can be used to control the torque as per Equation (3) (Makwana, 2021).

SRM suffers from high torque ripple problems, due to the discrete way of torque production. In this motor, when stator and rotor pole alignment approaches and departs causes a reduction in the average torque. Also, when commutate from one phase to another in sequence gives rise to torque ripples. The total torque generated by the motor is the summation of torques produced by the individual phase winding. Mathematically, steady state torque ripple in percentage is presented by Equation (4) (Kimpara et al., 2022):

$$\text{Torque ripple} = \frac{T_{max} - T_{min}}{T_{avg}} \times 100\% \tag{4}$$

Here, T_{max}, and T_{min} are the instantaneous values of maximum and minimum torque. T_{avg} is the average torque. Torque ripples can be reduced by the increase in the average torque produced by the SRM drive system using different converter topologies, control techniques, or structural changes.

2.2 SRM Converter Topology

In SR motor the power electronic converter works as a heart. The sort of power converter topology that is chosen will largely determine the size, cost, and performance of the SR motor drive. This power converter needs to fulfill some of the essential requirements to increase the overall performance of the drive for dynamic loading conditions. A few of the important requirements are:

- The drive system should be smaller and less expensive by using the fewest possible switches per phase in the converter unit.
- The input supply voltage for each motor phase winding must be its full value.
- The demagnetizing phase energy should be fed back to the source for regeneration purpose.
- Fault tolerance, steady state, and dynamic performance should be better.
- The converter unit must allow phase overlap control.
- The rating of the switches must be near the motor rating.

Most of the above-mentioned conditions are satisfied by the commonly used classical asymmetric bridge converter (ABC) topology except the first one mentioned. As classical ABC topology uses two switching devices per phase (8 switches, for a 4-phase motor) for higher phase motors, the size of the overall drive system increases considerably. Improved reduced switch converter topology uses one switch per phase was proposed by (Hu et al., 2019) with the named m-switch converter, for six-phase SRM and constant load torque. In this article, a similar topology is implemented for the dynamic load on a four-phase SR motor using the PI current control technique, and the results are compared with the classical asymmetric bridge converter.

3. Analysis of Converter Topologies

The operation of the classical ABC and improved converter is investigated here by utilizing the double-phase magnetization technique. The commutation process from one phase to another is depicted using switching pulses and mode diagrams. To comprehend the commutation process, only two phases are shown.

3.1 Classical Asymmetric Bridge Converter (2m Switch) Topology

Asymmetric bridge converter (ABC) preserves, eight switching devices and eight diodes for a 4-phase SRM (2m switches = 2*4= 8 switches) as shown in **Figure 2**.

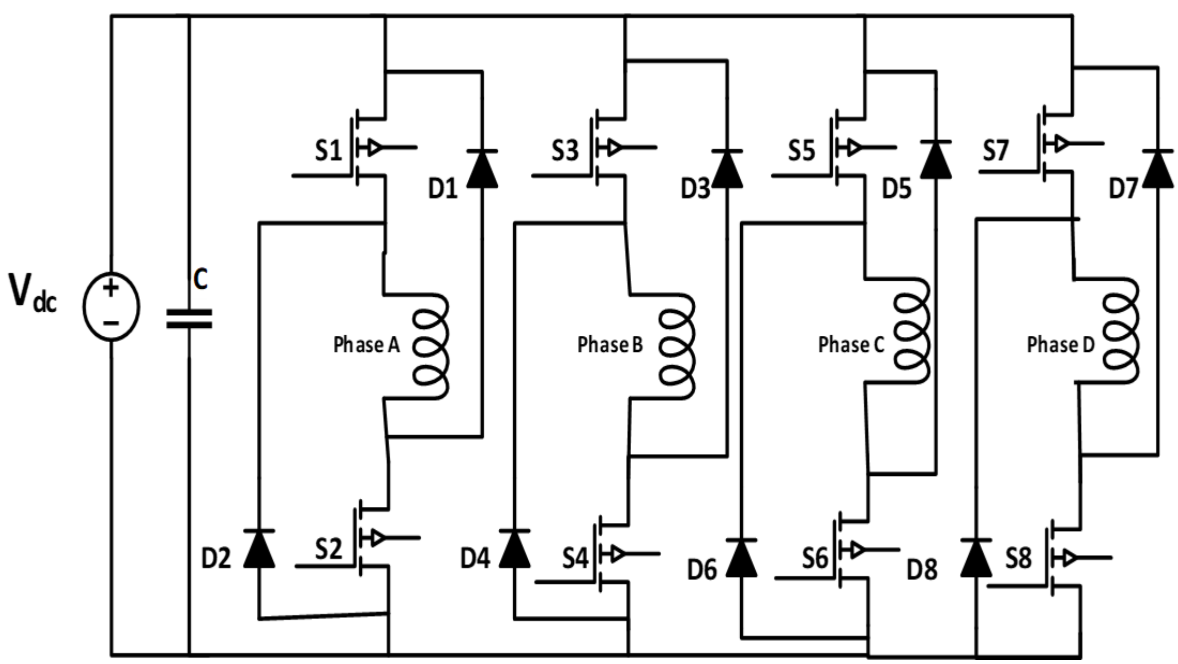

Figure 2. Asymmetric bridge converter topology for 4-phase SRM.

For high-speed operation each phase can be controlled separately. Both current and voltage control is possible (Agrawal and Bilgin, 2023), it provides the maximum control flexibility (Cai and Zhao, 2021). This classical converter topology provides decent competence for fault tolerance capability and can work on the limited capacity with any one switch damage (Xu et al., 2019). **Figure 3** shows the switching pulses to an asymmetric bridge converter using a double- phase magnetization scheme. The different commutation modes of ABC from A phase to B phase in double- phase magnetization is shown in **Figure 4**, for a four-phase motor. Each phase follows magnetization, demagnetization, and freewheeling. Different modes are explained here:

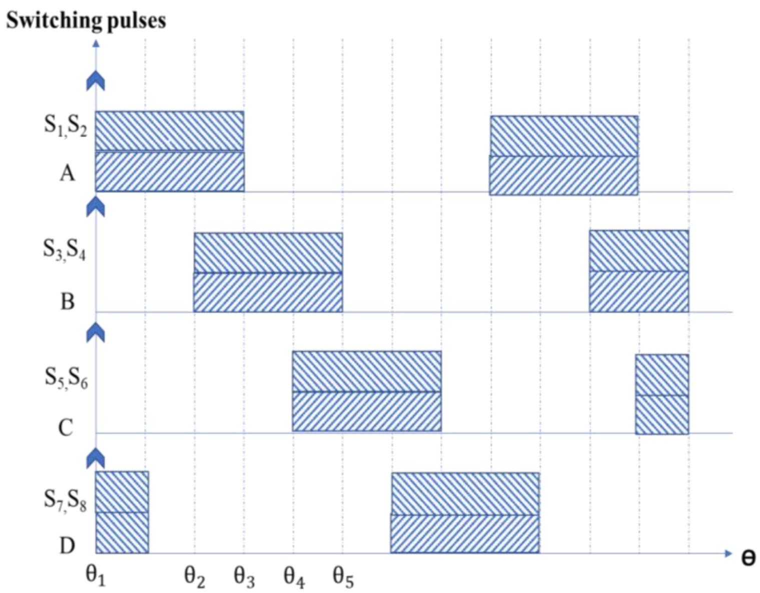

Figure 3. Switching pulses to an asymmetric bridge converter in double-phase magnetization.

***Mode*-1:** By activating switches S_1 and S_2 in **Figure 3**, phase A is first magnetized, which will conduct till θ_3. The conduction path in **Figure 4(i)** depicted that only phase A is activated.

***Mode*-2:** Switches S_3 and S_4 are turned on at θ_2 to magnetize the B phase. Both phases A & B will remain magnetized from θ_2 to θ_3 as per double-phase magnetization shown in **Figure 4(ii)**.

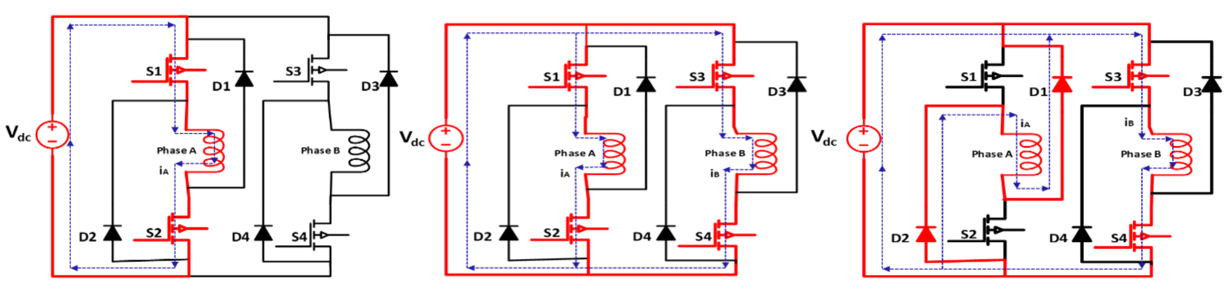

(i) Phase A singly magnetized (Double phase magnetization).

(ii) Phase A & B in magnetization.

(iii) Phase A demagnetization & B phase magnetization.

Figure 4. Commutation process in asymmetric bridge converter from phase A to B.

***Mode*-3:** Phase B remains singly excited after θ_3 till θ_4 only, and phase A is demagnetized as shown in **Figure 4(iii)**. After θ_4 next phase will be magnetized, to activate double-phase excitation, and the commutation process repeat.
Consider conduction duration for each phase winding is θ_p and for switching devices of that phase is θ_m then, it is given by Equation (5) for asymmetric converter (Hu et al., 2019):

$$\theta_p = \theta_m = \theta_3 - \theta_1 \tag{5}$$

Switching states Q_A during magnetization is represented by 1, for demagnetization -1, and for freewheeling 0. Based on this, the voltage equation for phase A in an asymmetric converter is represented by Equation (6) (Hu et al., 2019):

$$V_{phase_{(ABC)}} = \begin{cases} V_{dc} = 2V_m + V_A & Q_A = 1 \\ V_{dc} = -(2V_d + V_A) & Q_A = -1 \\ V_A + V_d + V_m & Q_A = 0 \end{cases} \tag{6}$$

Here, V_{dc} is the input DC voltage to the converter, and phase winding voltage is V_A for phase A. On-state voltage drop across the switch and diode are denoted by V_m and V_d, respectively.

3.2 Improved Reduced Switch Converter Topology

The improved reduced switch converter is rather similar to the classical ABC design, with a few alterations due to the usage of half the number of switches. This topology was first described by (Hu et al., 2019) for a six-phase SRM with a constant load. In this paper similar concept is applied for a four-phase SRM with dynamic load. **Figure 5** depicts the circuit diagram of an improved converter topology with only four switches and eight diodes for a four-phase SRM drive (Asati et al., 2024). As a number of switches are half that of the ABC, these four switches are shared by adjoining phase winding. Out of eight diodes, four diodes are shared by nearby phase windings, while the remaining four are coupled in series with each phase winding to prevent phase current reversal. When compared to the standard ABC topology, phase windings in this topology are not independent because they are attached to the neighboring phase winding terminal. This topology follows a different mode sequence than the ABC topology, which includes magnetization, freewheeling, and demagnetization. **Figure 6** shows the switching pulses of an improved converter topology with a double-phase magnetization scheme.

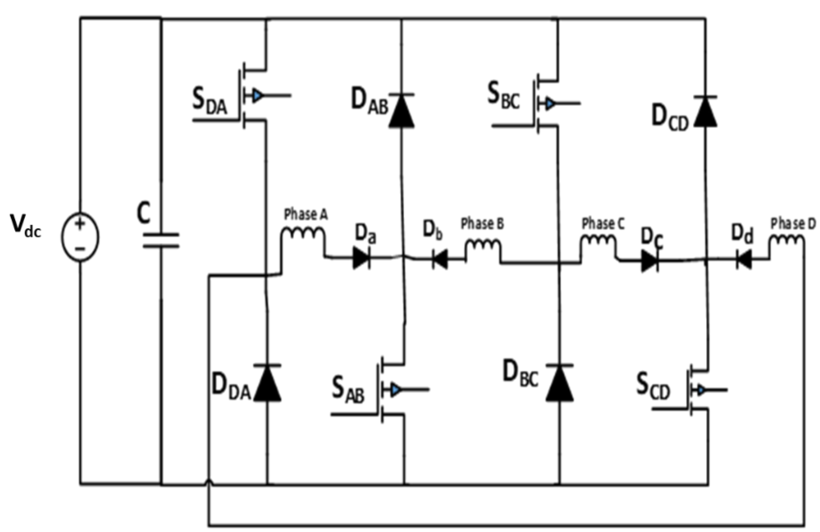

Figure 5. Improved reduced switch converter for 4-phase SRM.

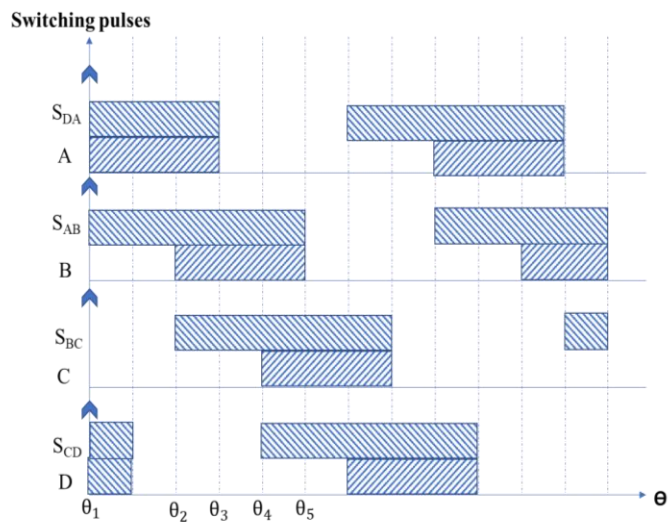

Figure 6. Switching pulses to improved reduced switch converter in double phase magnetization.

Commutation from A to B phase is represented via **Figure 7** in four modes as follow:

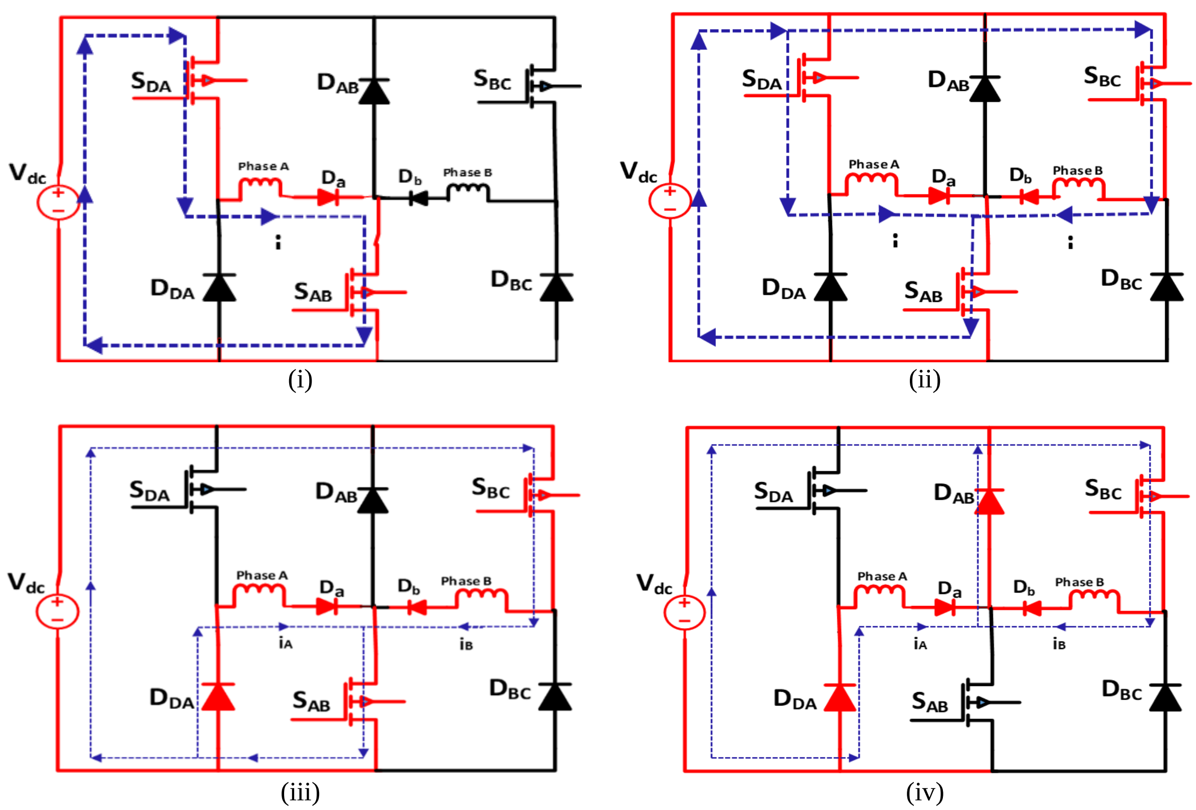

Figure 7. Commutation process in improved reduced switch converter from phase A to B. (i) Phase A singly magnetized, (ii) Phase A & B both in magnetization, (iii) A phase freewheeling & B phase magnetizing, (iv) A phase demagnetizing & B phase freewheeling.

***Mode*-1:** In **Figure 6** to magnetize phase A, switching pulses are applied to switch S_{AB} at θ_1, and S_{DA} is already conducting. This mode follows the magnetization of only phase A, current path for this magnetized phase A is shown in **Figure 7(i)**. Switch S_{AB} will conduct till θ_5.

***Mode*-2:** Switch S_{BC} will turn on at θ_2, this will magnetize phase B as well. Both phases A & B will remain magnetized in this mode from θ_2 to θ_3, similar to ABC topology as shown in **Figure 7(ii)**. Phase A remains magnetized from θ_1 to θ_3.

***Mode*-3:** In this mode, phase A freewheels from θ_3 to θ_5, which is different than the ABC as it follows demagnetization. Phase B is only magnetized in this mode from θ_2 to θ_5 as shown in **Figure 7(iii)**.

***Mode*-4:** Here, phase A is in demagnetization status until the phase current reduces to zero while phase B freewheels as shown in **Figure 7(iv)**. Now, the process will repeat for the remaining phases as well where; each phase will be magnetized, freewheeled, and then demagnetized in the sequence for improved converter topology.

Consider in the improved converter, the conduction duration of each switching device is θ'_m, and for phase winding θ'_p then it is given by Equation (7) (Hu et al., 2019):

$$\theta_p' = \theta_3 - \theta_1 \text{ and } \theta_m' = \theta_p + \theta_s \tag{7}$$

Here θ_s is called the step angle in SRM, which is represented by Equation (8) (Hu et al., 2019):

$$\theta_s = \frac{360^0}{m*N_r} \tag{8}$$

In SRM, N_r represents rotor pole number, and m presents number of phases. As per the motor specifications in **Table 1**, the value of θ_s in this paper is $(360^0/4*6) = 15^0$. Similar to ABC topology, phase winding voltage equation for an improved reduced switch converter is represented by Equation (9) (Hu et al., 2019):

$$V_{phase_{(reduced\ switch)}} = \begin{cases} \mathrm{V_{dc}} = 2\mathrm{V_m} + \mathrm{V_A} & \mathrm{Q_A} = 1 \\ \mathrm{V_A} + 2V_d + V_m & \mathrm{Q_A} = 0 \\ \mathrm{V_{dc}} = -(3\mathrm{V_d} + \mathrm{V_A}) & \mathrm{Q_A} = -1 \end{cases} \tag{9}$$

In this reduced switch topology; the winding voltage will not be zero, even when the current reduces to zero; till the current of the nearing phase becomes zero. Phase voltage of ABC topology has two voltage states $+V_{dc}$ and $-V_{dc}$ while, improved reduced switch topology has three states $+V_{dc}$, $-V_{dc}$, and 0 during the current dwelling.

3.3 Control Technique

To effectively regulate the phase currents of SRM, a hysteresis current controller is crucial. **Figure 8** shows the block diagram of PI-based hysteresis current controller to control the speed of the motor and keeping current in limit (Asati and Bankar, 2024). It is a simple, yet efficient, approach for attaining the required torque and speed characteristics. A hysteresis band is used to guarantee precise current regulation. By directly regulating the phase currents without the need for sophisticated motor models, this control technique allows quick dynamic response (Mittal et al., 2008; Kurian and Nisha, 2015). The iterative approach is used to determine the optimal values of the P and I parameters in the PI speed controller that involve a trade-off between responsiveness and stability. There is often an interaction between the P and I parameters. Increasing P can lead to an increase in overshoot but also make the system faster to change. However, introducing an appropriate amount of I can help in reducing steady-state error without exceeding overshoot or instability. By properly selecting P&I, a tailored response of the controller can be achieved to meet specific performance criteria such as settling time, overshoot, and steady-state error. In contrast to intelligent, complex control methods, hysteresis current control with a PI speed controller is the straightforward method. It maintains its stability in the face of intrinsic nonlinearities and variations in SRM parameters. Its key characteristics are simplicity of installation and quick transient response (Pratapgiri, 2016; Mittal and Panchal, 2023).

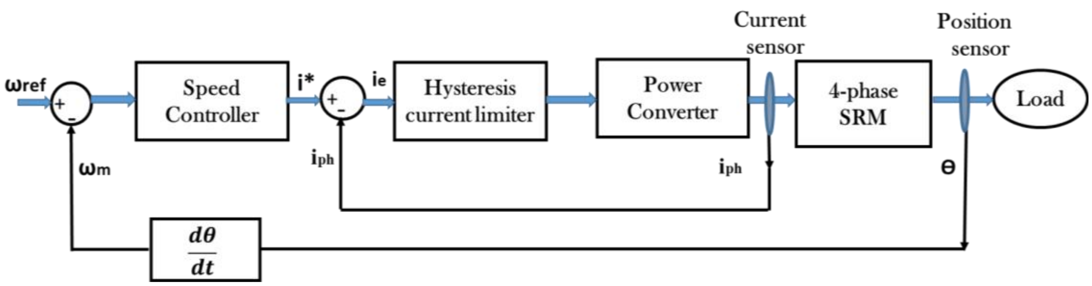

Figure 8. Block diagram of PI-based hysteresis current controller.

4. Comparative Analysis of Simulation Results

Analysis and comparison of classical Asymmetric bridge converter topology with improved reduced switch converter topology is performed in MATLAB/Simulink environment. An electric vehicle with a dynamic load weighing 1200 kg and a 7.5kW four-phase SRM model is taken from the simulink library. The 7.5kW SRM specification utilized in the simulation is presented in **Table 1**, and the vehicle road load parameters are shown in **Table 2**. PI-based hysteresis current control technique is adopted for both converter topologies. The motor rating in the simulation model allows for a maximum current of 35A in the phase windings; to simulate realistic conditions, the hysteresis band is set to 32A.To obtain optimum performance turn on and turn off angles are kept 30^0 & 45^0 respectively for a 4-phase SRM. The reference speed is set as 1000 RPM, and the DC voltage is 250V for both converters.

Table 1. Specification of four-phase switched reluctance motor.

Parameters	Value
Power rating (kW)	7.5
Type	8/6 pole
No. of phase	4
Stator resistance (ohm)	0.5
Friction (N-m. s)	0.02
Unaligned inductance (H)	9.15×10^{-3}
Aligned inductance (H)	145.9×10^{-3}
Saturated aligned inductance (H)	0.15×10^{-3}
Maximum current (A)	35
Maximum flux linkage (V.s)	0.9

Table 2. Parameters of vehicle road load.

Parameters	Value
Mass (kg)	1200
Rolling resistance coefficient (N)	2
Rolling and driveline resistance coefficient (N*s/m)	0.5
Aerodynamic drag coefficient (N*s^2/m^2)	0.389
Gravitational constant	9.81
Gradient	10
Initial position (m) and velocity (m/s)	0 and 0

Figure 9 depicts the performance waveforms, or the speed, current, and torque of the classical and improved converter topology. The same voltage, current references, and loading conditions are applied independently to each topology during simulation. As observed from **Figure 9(i)**, the initial peak current in both the converters is 32 A as it is limited by the hysteresis current controller. The steady-state maximum current in the improved converter is 8.5A due to the use of a serial diode in series with each phase winding. This series diode configuration aids in avoiding current reversal. While in ABC, this steady state maximum current is 18A. Though the phase winding current is lowered, each switch has to carry the current of two simultaneously conducting phases; that makes the switching losses almost equal in both the converter topologies.

Classical asymmetric bridge converter.

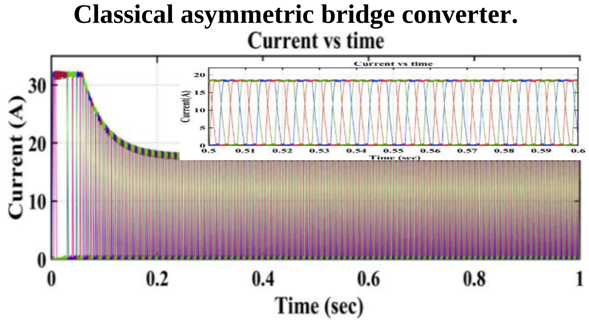

(i) Current vs. time

Improved reduced switch converter.

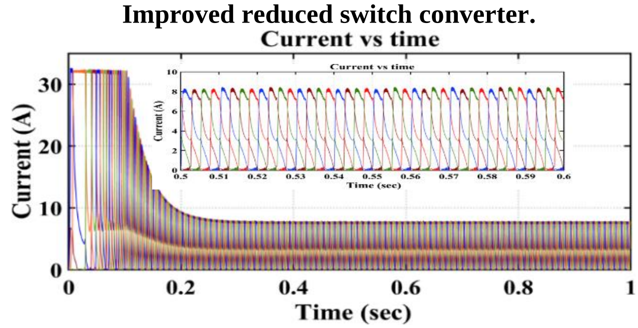

(i) Current vs. time

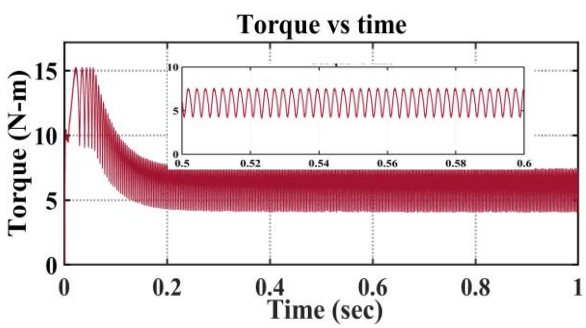

(ii) Torque vs. time

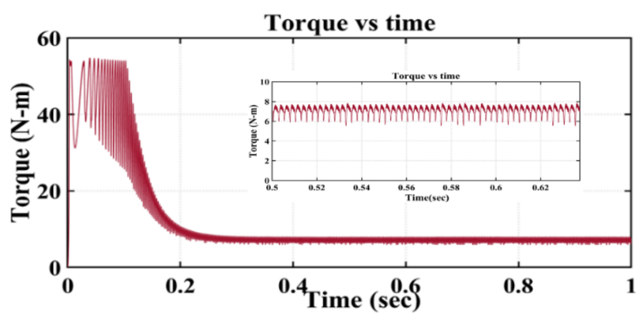

(ii) Torque vs. time

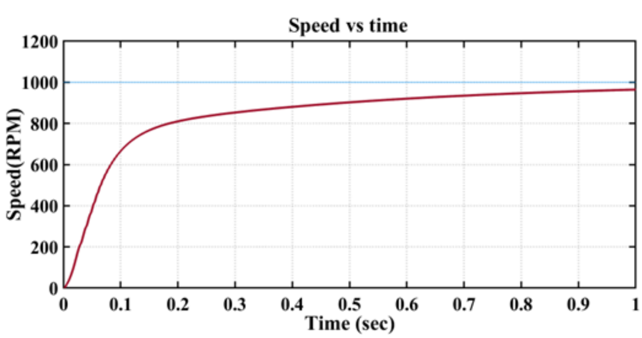

(iii) Speed vs. time

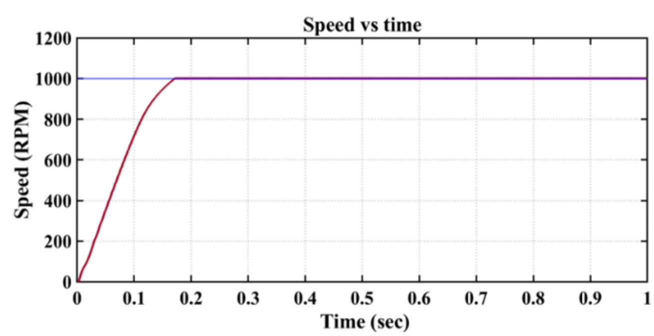

(iii) Speed vs. time

Figure 9. Simulation waveforms of a 4-phase SRM with asymmetric bridge and improved converter topology.

For classical topology, the phase winding voltage levels are $+\mathrm{V_{dc}}$ & $-\mathrm{V_{dc}}$ while in improved topology, there are three $+\mathrm{V_{dc}}$, $-\mathrm{V_{dc}}$ & zero. The comparison of torque waveforms in **Figure 9(ii)** shows that the average torque obtained is 5.75 N-m in the former and 6.5 N-m in the latter. The starting torque for classical ABC is only 15 N-m, however it is increased to 55 N-m in the improved topology. Torque ripple is calculated using Equation (4), and the value obtained for classical topology is 60.8%, whereas it is reduced to 30.7% in improved topology. Aside from providing good starting and average torque, the improved topology lowers the most critical problem of torque ripple by 50% when compared to ABC in SRM drives. As the conduction angle θ_{on} is advanced, an improved converter generates more torque than the ABC which helps in reaching a particular speed in less time. **Figure 9(iii)** depicts the speed waveform; the time required to reach steady state reference speed in a classical converter is more than one second, but it takes only 0.17 seconds in improved topology-driven motor. Freewheeling mode often produces a slower response than the demagnetization, this improved converter follows the commutation sequence as magnetization, freewheeling, and demagnetization, whereas in ABC, freewheeling and demagnetization are swapped after magnetization. The improved topology has better settling time than the classical topology while both the topologies are not undergoing any overshoot.

Table 3 summarizes the characteristics and conclusions of simulation results for a four-phase SRM drive employing classical and improved converter topologies. Switching devices dropped to half (only four for 4-phase SRM), contributing to the total size and cost reduction of the improved converter unit. The magnitude of the phase current in the improved converter was lowered due to the voltage drop in the serial diode. Improved average torque reduces torque ripple by around 50%, and increased average and starting torque are additional benefits of the improved converter.

Table 3. Comparison of converter topologies for 4-phase SRM.

Parameters	**Classical asymmetric bridge converter**	**Improved reduced switch converter**
No. of Switches	8	4
No. of Diodes	8	8
Average Torque	5.75 N-m	6.5 N-m
Starting Torque	15 N-m	55 N-m
Torque ripple	60.8%	30.7%
Steady state maximum Current	18A	8.5A
Speed Settling time	1 sec	0.17 sec
Commutation sequence	Magnetized ➔ demagnetized ➔ freewheel	Magnetized➔freewheel➔demagnetized
Cost	High	Low (Hu et al., 2019)
Winding Losses	High	Comparatively low

5. Conclusion

In this research work, the performance of a classical asymmetric bridge converter and an improved reduced switch converter for four-phase SRM with dynamic load is analyzed and compared. Classical ABC uses eight switches while improved topology operates with only four switches being shared by adjacent phases. Reduced switching devices to half, contribute to the overall size and cost reduction of converter unit. Both the converter topologies are studied using a double-phase magnetization scheme in different modes. According to the simulation results, the improved converter has a higher average and starting torque and uses a distinct commutation sequence magnetizing, freewheeling, and demagnetizing than the classical architecture. The reduced switch topology uses serial diodes in each phase, which helps to lower the steady-state phase current and maximize drive efficiency. The enhanced average torque mitigates the critical issue of torque ripple in SRM drive by fifty percent as compared to classical ABC. Study state speed attained by the motor using improved topology is also rapid and without overshoot. However; this converter alters the amount of current flowing through each phase of the motor by connecting switches to multiple phases of the motor. This presented research does not illustrate the effect of parameter changes during dynamic load, open and short circuit fault analysis, and prototype to validate the simulation results; these will be investigated in the subsequent research work.

Conflicts of Interest

The authors declare that they have no conflicts of interest

Acknowledgments

"The authors extend their appreciation to the Researchers Supporting Project at King Saud University, Riyadh, Saudi Arabia, for funding this research work through the project number RSP2023R278".

The authors extend their appreciation to the Researchers Supporting Project at Universiti Teknologi Malaysia (UTM), Malaysia (project no. UTMFR: Q.J130000.3823.23H05) for providing the facility for carrying out this research work.

The authors extend their appreciation to the Bharati Vidyapeeth (Deemed to be) University, College of Engineering, Pune, Maharashtra, India; Intelligent Prognostic Private Limited Delhi, India; Manipal Institute of Technology, Manipal Academy of Higher Education, Manipal, Karnataka, India and Ingenium Research Group, Universidad Castilla-La Mancha, 13071 Ciudad Real, Spain for providing technical and non-technical support for carrying out this research work."

For the correspondence, please contact the corresponding author(s) at MajedAlotaibi@ksu.edu.sa (Majed A. Alotaibi), hasmat@utm.my (Hasmat Malik), faustopedro.garcia@uclm.es (Fausto Pedro García Márquez).

References

Agrawal, A., & Bilgin, B. (2023). Determining the control parameters of a switched reluctance motor drive based on energy utilization. In *IEEE Access*, *11*, 59097-59107. https://doi.org/10.1109/access.2023.3284836.

Al-Amyal, F., Hamouda, M., & Számel, L. (2022) Performance improvement based on adaptive commutation strategy for switched reluctance motors using direct torque control. *Alexandria Engineering Journal*,*61*(11), 9219-9233. https://doi.org/10.1016/j.aej.2022.02.039.

Asati, R., & Bankar, D.S. (2024). Performance analysis of classical converter using different control strategies for switched reluctance motor with dynamic loading. In: Malik, H., Mishra, S., Sood, Y.R., Iqbal, A., Ustun, T.S. (eds) *Renewable Power for Sustainable Growth*. Springer, Singapore, pp. 457-467. https://doi.org/10.1007/978-981-99-6749-0_30.

Asati, R., Bankar, D.S., & Nehete, A.L. (2023). Comparative analysis of converter topologies used in switched reluctance motor for high torque electric vehicle application. *Materials Today: Proceedings*, *72*(3), 736-740. https://doi.org/10.1016/j.matpr.2022.08.497.

Asati, R., Bankar, D.S., Apte, A., Nehete, A.L., & Mandake, Y.B. (2024). Fuzzy controlled modified reduced switch converter for switched reluctance motor under dynamic loading. *Indonesian Journal of Electrical Engineering and Computer Science, 34*(1), 50-58. https://doi.org/10.11591/ijeecs.v34.i1.pp50-58.

Cabezuelo, D., Andreu, J., Kortabarria, I., Ibarra, E., & Garate, I. (2017). SRM converter topologies for EV application: State of the technology. In *2017 IEEE 26th International Symposium on Industrial Electronics* (pp. 861-866). IEEE. Edinburgh, UK. https://doi.org/10.1109/isie.2017.8001359.

Cai, J., & Zhao, X. (2021). An On-board charger integrated power converter for EV switched reluctance motor drives. *IEEE Transactions on Industrial Electronics, 68*(5), 3683-3692. https://doi.org/10.1109/tie.2020.2982112.

Cai, W., & Yi, F. (2016). An integrated multiport power converter with small capacitance requirement for switched reluctance motor drive. *IEEE Transactions on Power Electronics, 31*(4), 3016-3026. https://doi.org/10.1109/tpel.2015.2442924.

Ding, W., Li, K., Yuan, J., Li, J., & Du, C. (2023). Wireless power transmission-based in-wheel switched reluctance motor drive system with an x-type converter. *IEEE Transactions on Energy Conversion*, *38*(1), 450-462. https://doi.org/10.1109/tec.2022.3204179.

Fang, G., Scalcon, F.P., Xiao, D., Vieira, R.P., Gründling, H.A., & Emadi, A. (2021). Advanced control of switched reluctance motors (SRMs): A review on current regulation, torque control and vibration suppression. *IEEE Open Journal of the Industrial Electronics Society*, *2*, 280-301. https://doi.org/10.1109/ojies.2021.3076807.

Guan, M., Liu, C., Han, S., & Sun, X. (2020). Analysis of midpoint current characteristics for novel six-phase N+2 power converter in different working condition. *IEEE Access*, *8*, 105104-105117. https://doi.org/10.1109/access.2020.2999933.

Han, S., Diao, K., & Sun, X. (2021). Overview of multi-phase switched reluctance motor drives for electric vehicles. *Advances in Mechanical Engineering*, *13*(9), 1-18. https://doi.org/10.1177/16878140211045195.

Ho, C.Y., Wang, J.C, Hu, K.W, & Liaw, C.M. (2019). Development and operation control of a switched-reluctance motor driven flywheel. *IEEE Transactions on Power Electronics*, *34*(1), 526-537. https://doi.org/10.1109/tpel.2018.2814790.

Hu, Y., Wang, T., & Ding, W. (2019). Performance evaluation on a novel power converter with minimum number of switches for a six-phase switched reluctance motor. *IEEE Transactions on Industrial Electronics*, *66*(3), 1693-1702. https://doi.org/10.1109/tie.2018.2840480.

Indira, D., & Venmathi, M. (2023). Comparative assessment of converter topologies for switched reluctance motor drives. *IETE Journal of Research*, *69*(8), 5380-5398. https://doi.org/10.1080/03772063.2021.1977187.

Kimpara, M.L.M., Reis, R.R.C., Da Silva, L.E.B., Pinto, J.O.P., & Fahimi, B. (2022). A two-step control approach for torque ripple and vibration reduction in switched reluctance motor drives. *IEEE Access*, *10*, 82106-82118. https://doi.org/10.1109/access.2022.3195493.

Krishnan, R. (2001). *Switched reluctance motor drives: Modelling, simulation, analysis, design and applications*. CRC Press. ISBN: 9781315220062. https://doi.org/10.1201/9781420041644.

Kumar, P., Israyelu, M., & Sashidhar, S. (2023). A simple four-phase switched reluctance motor drive for ceiling fan applications. *IEEE Access*, *11*, 7021-7030. https://doi.org/10.1109/access.2023.3238068.

Kurian, S., & Nisha, G.K. (2015). Torque ripple minimization of SRM using torque sharing function and hysteresis current controller. In *2015 International Conference on Control Communication & Computing India* (pp. 149-154). IEEE. Trivandrum, India. https://doi.org/10.1109/iccc.2015.7432884.

Li, W., Cui, Z., Ding, S., Chen, F., & Guo, Y. (2022). Model predictive direct torque control of switched reluctance motors for low-speed operation. *IEEE Transactions on Energy Conversion*, *37*(2), 1406-1415. https://doi.org/10.1109/tec.2021.3131870.

Ma, M., Wang, Z., Yang, Q., Yang, S., & Zhang, X. (2019). Vector control strategy of a T-type three-level converter driving a switched reluctance motor. *Chinese Journal of Electrical Engineering*, *5*(4), 15-21. https://doi.org/10.23919/CJEE.2019.000023.

Mahmoud, S.M., El-Sherif, M.Z., Abdel-Aliem, E.S., & Nashed, M.N.F. (2013). studying different types of power converters fed switched reluctance motor. *International Journal of Electronics and Electrical Engineering*, *1*(4), 281-290. https://doi.org/10.12720/ijeee.1.4.281-290.

Makwana, J.A. (2021). *fundamentals of switched reluctance motor and drive (1st ed)*. Independently Published, Online. ISBN: 979-8547055058.

Mehta, N.D, Haque, A.M., & Patel, A. (2018). A review of switched reluctance motor converter topologies for automotive applications. *International Journal of Engineering Technology, Management and Applied Sciences*, *6*(2), 7-17.

Mittal, U. (2023). Detecting hate speech utilizing deep convolutional network and transformer models. In *2023 International Conference on Electrical, Electronics, Communication and Computers* (pp. 1-4). IEEE. Roorkee, India. https://doi.org/10.1109/elexcom58812.2023.10370502.

Mittal, U., & Panchal, D. (2023). AI-based evaluation system for supply chain vulnerabilities and resilience amidst external shocks: An empirical approach. *Reports in Mechanical Engineering, 4*(1), 276-289. https://doi.org/10.31181/rme040122112023m.

Mittal, U., Yang, H., Bukkapatnam, S.T.S., & Barajas, L.G. (2008). Dynamics and performance modelling of multi-stage manufacturing systems using nonlinear stochastic differential equations. In *2008 IEEE International Conference on Automation Science and Engineering* (pp. 498-503). IEEE. Arlington, VA. https://doi.org/10.1109/coase.2008.4626530.

Padmanaban, L.A., & Saravanan, P. (2023). Design, analysis and comparison of switched reluctance motors for electric vehicle application. *Automatika*, *64*(2), 239-247. https://doi.org/10.1080/00051144.2022.2140388.

Pires, V.F., Pires, A.J., Cordeiro, A., & Foito, D. (2020). A review of the power converter interfaces for switched reluctance machines. *Energies*, *13*(13), 3490. https://doi.org/10.3390/en13133490.

Pollock, C., & Williams, B.W. (1990). Power convertor circuits for switched reluctance motors with the minimum number of switches. *IEE proceedings B (Electric Power Applications), 137*(6), 373-384. https://doi.org/10.1049/ip-b.1990.0046.

Pratapgiri, S (2016) Comparative analysis of hysteresis current control and direct instantaneous torque control of switched reluctance motor. In *2016 International Conference on Electrical, Electronics, and Optimization Techniques* (pp. 2856-2860). IEEE. Chennai, India.

Rana, A.K., & Teja, A.V.R. (2020). A modular converter topology with fast discharging and regenerative capability for any n-phase SRM drive. *In IECON 2020: The 46th Annual Conference of the IEEE Industrial Electronics Society* (pp. 1175-1180). IEEE. Singapore. https://doi.org/10.1109/iecon43393.2020.9255370.

Riyadi, S. (2018). Analysis of C-dump converter for SRM drives. In *International Conference on Electrical Engineering and Informatics* (pp. 179-184). IEEE. BandaAceh, Indonesia. https://doi.org/10.1109/iceltics.2018.8548791.

Son, I., Lukman, G.F., Shah, M.H., Jeong, K.I., & Ahn, J.W. (2021). Design considerations and selection of cost-effective switched reluctance drive for radiator cooling fans. *Electronics*, *10*(8), 917. https://doi.org/10.3390/electronics10080917.

Subbamma, M.R., Madhusudhan, V., & Anjaneyulu, K.S.R.. (2016). SRM speed control with various converter topologies. *International Journal of Advanced Research in Electrical, Electronics and Instrumentation Engineering*, *5*(6), 4939-4951.

Sun, Q., Wu, J., Gan, C., & Guo, J. (2019). Modular full-bridge converter for three-phase switched reluctance motors with integrated fault-tolerance capability. In *IEEE Transactions on Power Electronics*, *34*(3), 2622-2634. https://doi.org/10.1109/tpel.2018.2846539.

Sun, X., Zhu, Y., Cai, Y., Xiong, Y., Yao, M., & Yuan, C. (2023). Current fault tolerance control strategy for 3- phase switched reluctance motor combined with position signal reconstruction. In *IEEE Transactions on Energy Conversion*, *38*(3), 1679-1690. https://doi.org/10.1109/tec.2023.3239525.

Xu, S., Chen, H., Yang, J., & Dong, F. (2019). Performance evaluation and reliability enhancement of switched reluctance drive system by a novel integrated power converter. In *IEEE Transactions on Power Electronics*, *34*(11), 11090-11102. https://doi.org/10.1109/tpel.2019.2900328.

Yi, F., & Cai, W. (2016a). A quasi-Z-source integrated multiport power converter as switched reluctance motor drives for capacitance reduction and wide-speed-range operation. *IEEE Transactions on Power Electronics*, *31*(11), 7661-7676. https://doi.org/10.1109/tpel.2016.2521351.

Yi, F., & Cai, W. (2016b). Modeling, control, and seamless transition of the bidirectional battery-driven switched reluctance motor/generator drive based on integrated multiport power converter for electric vehicle applications. *IEEE Transactions on Power Electronics*, *31*(10), 7099-7111. https://doi.org/10.1109/tpel.2015.2510286.

Zhao, S., & Ye, C. (2023). Research on low switching loss control strategy of high-speed FESS based on NPC three-level converter. *IEEE Transactions on Transportation Electrification*, *9*(1), 1403-1415. https://doi.org/10.1109/tte.2022.3193737.